Hindawi
International Journal of Chemical Engineering
Volume 2024, Article ID 5432109, 18 pages
https://doi.org/10.1155/2024/5432109

Research Article

Impact of Aqueous Extract Artemisia Herba-Alba Leaves as a Green Inhibitor against Acid Activation of 2024 Aluminum Alloy

Nacer Hechiche,[1] Gérald Culioli,[2] Abdelaziz Kadri,[1] Dalila Boughrara,[1] Amar Saal,[3] and F. Xavier Perrin[4]

[1]*Materials Physics and Chemistry Laboratory, Mouloud Mammeri University, Tizi-Ouzou, Algeria*
[2]*Mediterranean Institute of Marine and Terrestrial Biodiversity and Ecology, UMR CNRS-IRD, Aix-Marseille University, Avignon, France*
[3]*Laboratory of Theoretical Computational Chemistry and Photonics, USTHB, Algiers, Algeria*
[4]*MAPIEM Laboratory, Toulon University, La Garde, France*

Correspondence should be addressed to F. Xavier Perrin; perrin@univ-tln.fr

Received 4 December 2023; Revised 9 February 2024; Accepted 12 March 2024; Published 22 March 2024

Academic Editor: Sébastien Déon

Copyright © 2024 Nacer Hechiche et al. This is an open access article distributed under the Creative Commons Attribution License, which permits unrestricted use, distribution, and reproduction in any medium, provided the original work is properly cited.

This work is part of the development of new bio-sourced corrosion inhibitors from an abundant resource that can replace conventional synthetic inhibitors that are harmful to both human health and the environment. The corrosion inhibition performance of an aqueous extract of *Artemisia herba-alba* on the corrosion of 2024 aluminum alloy in a 1 M hydrochloric acid solution is investigated by weight loss method, electrochemical (linear polarization, potentiodynamic polarization, and electrochemical impedance spectroscopy) and SEM techniques. The extract shows excellent corrosion-inhibiting properties on aluminium alloy with a maximum inhibition efficiency of 93% at 0.6 g/L. The adsorption of the natural extract obeys the extended Langmuir isotherm equation adsorption model for multicomponent systems. Temperature studies show that the efficiency of the extract decreases with increasing temperature and that the corrosion activation energies increase in the presence of the extract. Liquid chromatography/high resolution mass spectrometry is used to identify the chemical constituents of the natural extract, and the most abundant phytochemicals for each subclass of metabolite are investigated using density functional theory (DFT) calculations. This study paves the way for further development of a plant that is particularly abundant in the desert regions of North Africa and has until now been used mainly for food for livestock and for pharmaceutical applications.

1. Introduction

Aluminum and its alloys are still attracting the attention of the scientific community because of their high mechanical strength, low cost, low density, and good machinability [1]. They have been widely used in various industrial applications such as construction, transportations, electronics, packaging, storage, and stock-keeping. Alloying aluminum aims to increase its strength by forming intermetallic particles (IMPs). The presence of a protective oxide layer gives Al and its alloys their inherent corrosion resistance [2]. In highly acidic and alkaline media (below pH 4 and above pH 8.5), the solubility of the oxide film increases at room temperature, and heavy corrosion is observed [3].

It is commonly recognized that the corrosion of aluminum in an acidic environment occurs by the migration of ions through the oxide layer [4], followed by multistep dissolution involving chemical reactions of chloride ions with Al [5]. Cabot et al. [6] have reported from potentiodynamic and galvanostatic transient techniques that the corrosion of aluminum in concentrated HCl solutions takes place through the formation and dissolution of a defective

oxohydroxide film. Pitting with intergranular fissuring attack has been observed in aerated solutions but no pits have developed in deaerated solutions. Hydrochloric acid solutions are used in several processes, such as acid pickling [7] and chemical and electrochemical etching [8] of aluminum and its alloys. The introduction of corrosion inhibitors is an effective way to reduce the corrosion rate of Al and its alloys in such aggressive solutions [9]. Given the known acidic pH inside pits and crevices [10], corrosion inhibition tests in an acidic chloride medium can also be used to evaluate the inhibitor's capacity to repassivate or reduce pit or crevice growth.

Organic compounds that are used as corrosion inhibitors frequently have O, N, S, and/or P atoms in their chemical structure that act as binding sites for the adsorption on the surface of aluminum. Many of these inhibitors are synthetic compounds, which are extremely hazardous to human health and the environment. The use of natural compounds is an interesting alternative as a sustainably sourced and environmentally friendly substitute for synthetic inhibitors [11–16]. Many groups of natural compounds have been considered potential corrosion inhibitors for aluminum and its alloys. The greater part of these studies have involved plant extracts. Plant materials such as leaves [17], seeds [18], barks [19, 20], pulp and fruit juice [21], husk and flowers [22], roots [23], and exudate gums [24] were commonly used to prepare such extracts. Corrosion inhibition by plant extracts in acidic solutions generally occurs via physisorption of their chemical components on the Al surface [24–29].

Artemisia herba-alba (AHA) is a shrub commonly found in the Mediterranean region. In Algeria and North Africa, AHA covers huge territories estimated at over ten million hectares. Artemisia genus is abundant in tannins, flavonoids, and terpenoids, which offer its species therapeutic and aromatic qualities, according to earlier phytochemical studies [30, 31]. In particular, a wide range of biological activities have been described for Artemisia herba-alba extracts, among which antioxidant, antibacterial, cytotoxic, and pesticidal activities can be mentioned [32].

Several studies on the composition of AHA oil have been reported, and several chemotypes have been observed [33]. The essential oil from AHA with β-thujone [34], 1,8-cineole [35], chrysanthenone [36], or camphor [37] as major components has shown good inhibitive properties for the corrosion of steel [34, 36], stainless steel [35], and aluminum [37] in an acidic environment. It must be noted that the camphor molecule is present in significant proportions (16–25%) in all the AHA oils studied. The inhibitory activity of aqueous and methanolic extracts of AHA against steel corrosion in an acidic medium has been the subject of more recent studies [38]. Phenolic compounds including some flavonoids, tannins, and phenolic acids have been identified in the aqueous extract of AHA leaves. From DFT investigations, it has been deduced that the good inhibitory properties of aqueous extract of Artemisia herba-alba (AHAE) on the corrosion of mild steel in 1M HCl could be due to one of the main components of this extract, 3-O-caffeoylquinic acid [38]. As far as we are aware, there has been no research on how AHAE can prevent the corrosion of aluminum or its alloys.

Herein, we report the results of a study on the inhibitory properties of AHAE on the corrosion of 2024 aluminum alloy in 1M HCl solution using weight loss measurement and electrochemical techniques. SEM observations were also performed to highlight the inhibitory action of AHAE on aluminum alloy while the gross chemical composition of this extract was studied by liquid chromatography tandem mass spectrometry (LC-MS/MS) analysis. DFT calculations were performed in order to compare the reactivities and bonding sites of the most abundant molecules representative for each subclass of metabolite identified by LC-MS/MS. The present work is aimed at developing new low-price, bio-sourced, and eco-friendly inhibitors for the corrosion of aluminum and its alloys in acidic solution.

2. Materials and Methods

2.1. Materials. The study was conducted on 2 mm thick Al 2024-T3 aluminum alloy sheets (wt. %: Cr 0.1; Si 0.5; Ti 0.15; Fe 0.5; Zn 0.25; Mn 0.3–0.9; Mg 1.2–1.8; Cu 3.8–4.9; others 0.05–0.15; Al balance) cut to 30 mm by 10 mm coupons.

2.2. Collection of Plant Material and Preparation of AHAE. The aerial parts (leaves) of *Artemisia herba-alba* (AHA) used in this study were collected in May 2019 in Sidi Hadjeres (locality of Msila, Algeria). The collection site (35°40′24.8″N, 4°04′16.7″E, 504 m above sea level) was characterized by a semiarid climate with an annual average temperature of 23°C and rainfall of 18.7 mm. The plant was properly washed under running water, rinsed with distilled water, and then placed into an oven set to 60°C for drying. In a second step, the plant is reduced to powder using an electric grinder.

The AHAE was prepared as follows: 3 g of AHA powder was macerated with agitation in 300 mL of distilled water for 72 h. The mixture was filtered (Whatman N°1), and the filtrate was freeze-dried with a Heto PowerDry LL 1500 (Thermo) freeze dryer. The extraction procedure yielded 0.6 g of aqueous extract, corresponding to an extraction yield of 20%. The powdered extract was added to an aqueous solution of 1M HCl in concentrations ranging from 0.1 to 0.6 g/L.

2.3. LC-MS/MS Analysis of AHAE. LC-MS/MS analysis was used for the identification of the aqueous extract of AHA. The chromatographic system (Dionex Ultimate 3000 Rapid Separation; Thermo Fisher Scientific, Waltham, MA, USA) was equipped with a photodiode array detector and a QToF mass spectrometer (Impact II; Bruker Daltonics, Mannheim, Germany). Separations were performed on a reverse-phase analytical column (column: 150 × 2.1 mm, 1.7 μm, Kinetex Phenyl-Hexyl and precolumn: SecurityGuard cartridge; Phenomenex, Torrance, CA, USA) maintained at 40°C. The flow rate, the injection volume, and the autosampler temperature were set at 0.5 mL/min, 5 μL, and 4°C, respectively. Mobile phases were composed of water (Eluent A) and acetonitrile (Eluent B) (Chromasolv; Sigma-Aldrich,

Saint-Louis, MO, USA) acidified with formic acid (0.1% (v/v); ultra grade; Thermo Fisher Scientific). The elution gradient began with 5% B for 2 min; it was then increased to 100% B in 8 min (linear ramp), and this final composition was maintained for 4 min. The reconditioning of the column was achieved by returning to the initial conditions (5% B) in 0.01 min (linear ramp) and during 1.99 min, leading to a total duration of the analysis of 16 min. The mass spectrometer was used with a capillary voltage set at 4500 V in positive mode. The nebulizing gas (N_2) pressure was set at 0.4 bar, the drying gas (N_2), flow at 4 L/min, and the drying temperature at 180°C. A mass range from *m/z* 50 to *m/z* 1200 (mass resolving power: 25,000) was used, and the frequency was set at 2 Hz. Internal mass calibration was done through the automatic injection of a solution of formate/acetate forming clusters before each sample. The mass spectrometer was calibrated with this same solution at the beginning of the injection sequence. MS/MS data were obtained thanks to collision-induced dissociation (CID; 5 main precursor ions) with a collision energy ranging from 18 to 45 eV depending on the *m*/*z* values.

2.4. Weight Loss Measurements. Prior to measurements, the 2024 aluminum alloy samples were wet-polished with up to 1200 grade SiC paper, followed by an ultrasonic stirring in absolute ethanol and a cold air-dried step. The freshly polished samples were weighed on an OHAUS analytical balance (0.1 mg) prior to and after having been imposed for a period of time in the 1 M HCl solution with and without AHA extract additions. After immersion in the corrosive medium, samples were rinsed with distilled water and dried under a stream of nitrogen before weighing. The temperature of the solution was maintained constant (temperature range of 298 to 328 K) using a thermostated water bath. It should be mentioned that the tests were run three times, and excellent repeatability was shown. Preliminary tests carried out at the maximum concentration of the extract (0.6 g/L) over a period of 6 hours of immersion showed a linear loss of mass with time, indicating a rapid adsorption-desorption equilibrium and stability of the anticorrosion activity of the extract over the 0–6 h time range. Following this observation, the following measurements were taken after 1 hour of immersion in the corrosive medium.

The corrosion rates expressed as loss of mass per unit of exposed surface and time have been converted to loss of thickness per unit of time (mm/year) by taking into account the density of the AA2024 alloy ($d = 2.78\ \mathrm{g/cm^3}$).

The inhibition efficiency, η_w, was calculated from the following equation:

$$\eta_w\,(\%) = 100 \times \frac{\mathrm{CR}^0 - \mathrm{CR}}{\mathrm{CR}^0}, \tag{1}$$

where CR^0 and CR are the values of the corrosion rate in the absence and the presence of the inhibitor, respectively.

2.5. Electrochemical Measurements. The electrochemical tests were carried out in a conventional three-electrode cell, with a platinum counter electrode, a saturated calomel electrode (SCE) as a reference electrode, and a 2024 aluminum alloy sample as a working electrode. The samples were embedded in bakelite (exposed area 1 $\mathrm{cm^2}$), abraded with various grades of silicon carbide papers up to 1200 grade, and ultrasonically cleaned in ethanol before analysis. An Autolab potentiostat PGSTAT-30 driven by GPES and FRA 4.9 Software (Eco Chemie, the Netherlands) was used for the electrochemical measurements. Electrochemical impedance spectroscopy (EIS), polarization resistance, and potentiodynamic measurements were carried out on separate samples after 1 hour of immersion in the corrosive medium to ensure that stationary conditions had been reached. EIS patterns were recorded at the OCP in the frequency range of 10 kHz to 0.01 Hz with a signal amplitude of 10 mV. The Boukamp's EQUIVCRT program was used for EIS data modelling and curve fitting [39].

In order to determine the polarization resistance, the potential of the 2024 aluminum alloy electrode was linearly swept over a scan range of −10 mV to +10 mV, with respect to open circuit potential (OCP), at a scan rate of 0.1 mV/s. Potentiodynamic polarization tests were recorded over a scan range of −300 mV to +300 mV, with respect to OCP, at a scan rate of 1 mV/s. All electrochemical measurements were carried out at least in duplicate.

2.6. Surface Analysis. The morphological observations of the 2024 aluminum alloy surface were conducted using a ZEISS-EVO15 scanning electron microscope prior to and following their immersion for 1 h at 25°C in a stagnant 1M HCl solution with and without AHAE.

2.7. Molecular Modelling. The molecular electronic properties of the major molecules in the extract were calculated using density functional theory (DFT) to assess their adsorption bonding characteristics and abilities. All geometry optimizations and quantum chemical calculations were performed using the hybrid B3LYP functional with a polarized double zeta basis set 6–31 + G (d). The chemical descriptors including the highest occupied molecular orbital energy, E_{HOMO}; the lowest unoccupied molecular orbital energy, E_{LUMO}; electronegativity, $\chi = -0.5(E_{\mathrm{HOMO}} + E_{\mathrm{LUMO}})$ and global hardness, $\eta = -0.5(E_{\mathrm{HOMO}} - E_{\mathrm{LUMO}})$ were reported. [40].

3. Results and Discussion

3.1. Weight Loss Measurements. The weight loss results such as the corrosion rate and the inhibition efficiency of 2024 aluminum alloy immersed in the 1M HCl solution containing different concentrations of AHAE are summarized in Table 1. It can be seen from Table 1 that the corrosion rate of the 2024 aluminum alloy gradually decreases with increased AHAE concentration. This can be explained by the increase in surface coverage by adsorption of the molecules of the extract on the active sites of the alloy surface. A maximum value of inhibition efficiency of 93.1% is achieved at 0.6 g/L of AHA extract which shows that AHA extract is a good inhibitor of 2024 aluminum alloy corrosion in 1M

Table 1: Weight loss data for AA2024 in 1.0 M HCl at different concentration of AEAHA and KI at 298K.

C_{AHA} (g/L)	CR (mm/year)	η_w (%)
Blank	396.7	
0.1	115.4	70.9
0.2	60.6	84.7
0.4	34.0	91.4
0.6	27.2	93.1

HCl medium, in particular by comparing these IE values with those obtained with other natural extracts. For example, the inhibitive effects of 1.5 g/L Mentha pulegium [41] and 0.75 g/L Thymus algeriensis [25] acidic aqueous extracts on 2024 aluminum alloy in 1M HCl attained 61% and 78.7%, respectively.

3.2. Open Circuit Potential (OCP). Figure 1 shows the evolution of the open circuit potential, OCP, with the immersion time in a 1M hydrochloric acid solution with and without the addition of the AHA extract at different concentrations. OCP values continuously evolve towards anodic values, with a rapid increase during the first 10 minutes of immersion followed by a slower increase thereafter. The same evolution is observed for the solution containing the AHE extract but with a strong shift of the OCP values in the cathodic direction compared to the blank solution. The potential evolution of the potential is opposite to that generally observed with aluminum. The change of OCP towards more negative values with aluminum is ascribed to the dissolution of the air pre-formed oxide film in the HCl solution [42]. The anodic evolution of the potential observed with the 2024 aluminum alloy is therefore linked to the particular microstructure of this alloy but not exclusively since the same type of evolution has been reported for an Al 6061 alloy [43]. Such an anodic evolution of the potential is generally associated with the formation of a protective passive film at the alloy surface [43]. The shift of the potential towards anodic values could have another explanation in connection with a selective dissolution of the less noble elements of the alloy and an enrichment of the surface in copper, as it was demonstrated during the acid deoxidizing of 2024 aluminum alloy [44].

3.3. Polarization Behaviour. The linear polarization resistance (LPR) method easily yields the polarization resistance, R_P from the current-voltage i-E characteristics in the vicinity of the corrosion potential. [45] R_P is basically the slope of the potential-current plot at the corrosion potential E_{corr}

$$R_p = \left(\frac{dE}{dI}\right)_{E_{corr}}. \quad (2)$$

LPR plots for 2024 aluminum alloy in blank solution and in the presence of AHA extract are shown in Figure 2. It can be noticed that the slope of the i-E curve for 2024 aluminum alloy is much lower in the presence of AHA extracts than in

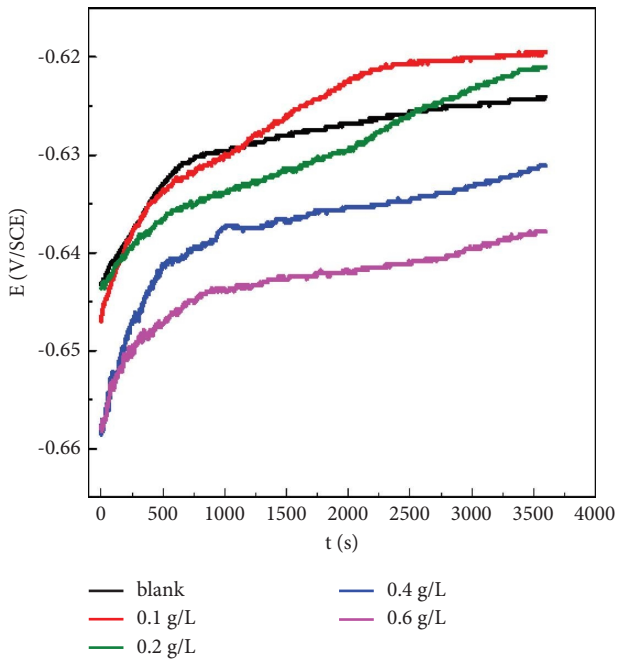

Figure 1: Variation of the open circuit potential of Al 2024 alloy electrode in 1.0 M HCl in the presence and absence of different concentration of AHA extract at 298 K.

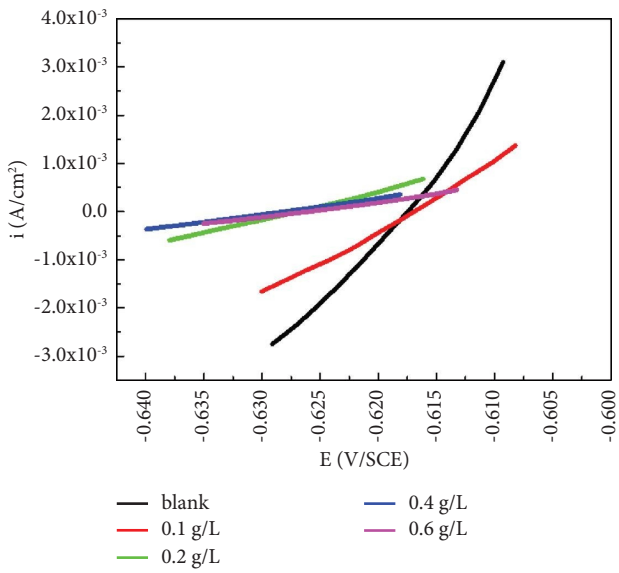

Figure 2: Current-voltage characteristics in the vicinity of the corrosion potential of Al 2024 alloy electrode in 1.0 M HCl in the presence and absence of different concentration of AHA extract at 298 K.

the blank solution. That is to say, the value of the polarization resistance increases in the presence of AHA extract. The inhibition efficiency was deduced from R_P values using the following relationship:

$$\eta_{LPR}(\%) = \frac{Rp - R_p^0}{R_p^0} \times 100, \quad (3)$$

where R_p^0 and R_p are the polarization resistance for the uninhibited and inhibited systems, respectively.

The values of polarization resistance, R_P, and inhibition efficiency at different AHAE concentrations are given in Table 2. The results indicated an increase in the effectiveness of the inhibition with the concentration of AHA extract, in agreement with the gravimetric data.

Figure 3 shows the potentiodynamic polarization curves of 2024 aluminum alloy after 1 h of immersion in 1 M HCl containing different concentrations of AHA extract at 25°C. The corrosion current density (j_{corr}) was determined by extrapolation of the cathodic Tafel line to the corrosion potential since the anodic polarization curve has not a well-defined linear portion [2]. The inhibition efficiency (η_P) was calculated at different concentrations of AHA extract using the following equation:

$$\eta_P(\%) = \frac{j_{corr}^0 - j_{corr}}{j_{corr}^0} \times 100, \quad (4)$$

where j_{corr}^0 and j_{corr} are the corrosion current density in the absence and presence of AHAE, respectively.

Several electrochemical kinetic parameters including corrosion potential, E_{corr}, corrosion current density, j_{corr}, cathodic Tafel slope, b_c, and inhibition efficiency, η_P determined from potentiodynamic polarization measurements (PPM) are listed in Table 3. The high anodic current values (>10 mA·cm^{-2} current density values are reached at overpotentials larger than 20 mV) reflect the dissolution of the unstable oxide layer under these strongly acidic conditions (pH = 0).

The addition of AHA extract to the acidic medium does not greatly affect the anodic part of the polarization curve at a low concentration of AHA extract. However, a significant decrease in the anodic current is still observed for the highest concentration of AHA extract (0.6 g/L). The sharp rise in the anodic current at a potential of −0.44 V/SCE could be due to a desorption of the molecules of the extract at a high overpotential. On the other hand, AHA extract strongly affects the cathodic part of the polarization curve. In fact, there is a shift towards lower cathodic current densities, and the addition of AHA extract shifts E_{corr} towards more negative values with increasing the AHAE concentration. Therefore, the hydrogen evolution process is inhibited in the presence of AHA extract. From Table 3, it is seen that the cathodic slope b_c decreased significantly in the presence of AHA extract in the acid medium which indicates that AHA extract alters the hydrogen evolution mechanism. AHA extract therefore acts mainly as a cathodic inhibitor but also with a significant anodic inhibitory effect at the extract's highest concentrations.

3.4. Electrochemical Impedance Spectroscopy Measurements. The EIS plots of 2024 aluminum alloy samples in quiescent 1 M HCl solutions in the absence and presence of AHA extract at different concentrations are shown in Figures 4 and 5.

The Nyquist plots in Figure 4 exhibit a capacitive loop at high frequency (HF) followed by two inductive loops at low frequencies (LF). This type of diagram is frequently reported

Table 2: Polarization resistance and inhibitor efficiencies for AA2024 in 1M HCl at different concentration of AEAHA at 298K.

C_{AHA} (g/L)	R_p (Ω cm^2)	η_{LPR} (%)
Blank	5.75	—
0.1	12.82	55.1
0.2	18.04	68.1
0.4	32.14	82.1
0.6	34.56	83.4

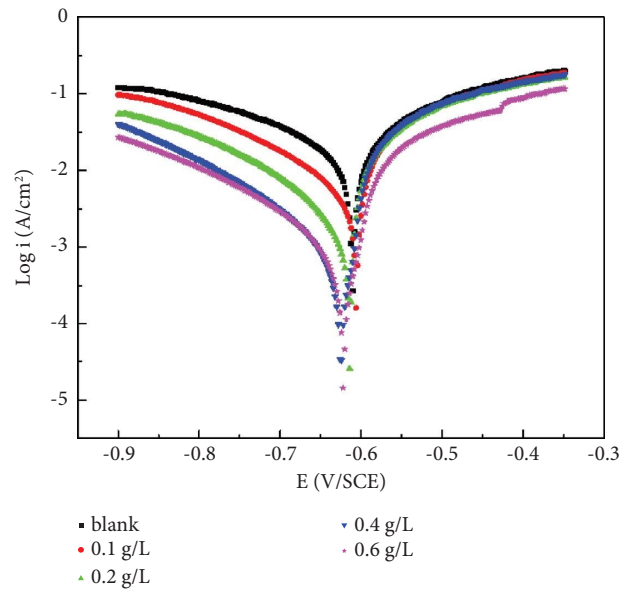

Figure 3: Polarization curves of Al 2024 alloy electrode in 1.0 M HCl in the presence and absence of different concentration of AHA extract at 298 K.

Table 3: Potentiodynamic polarization parameters for AA2024 in 1.0 M HCl without and with different concentrations of AEAHA at 298K.

C_{AHA} (g/L)	E_{corr} (V/SCE)	b_c (mV dec^{-1})	j_{corr} (mA cm^{-2})	η_P (%)
Blank	−0.610	300	20.00	—
0.1	−0.605	211	6.31	68.5
0.2	−0.614	184	2.82	85.9
0.4	−0.626	196	1.70	91.5
0.6	−0.623	205	1.52	92.4

for aluminum and its alloys in concentrated HCl media [42, 46]. The HF capacitive loop has been ascribed to the formation of the oxide layer including the formation of oxychloride complexes [42] or to the oxide layer itself [47, 48]. The inductive loop is always observed in acidic solutions, but it is not clearly understood. It is often attributed to bulk or surface relaxation of species in the oxide or to adsorbed intermediates such as H^+ [46]. The inductive loop for Al in the pitted active state can also be related to surface area modulation or salt film property modulations [47]. The addition of AHA extract does not change the shape of the impedance diagrams but increases the size of the capacitive and inductive loops. From the Bode modulus plot

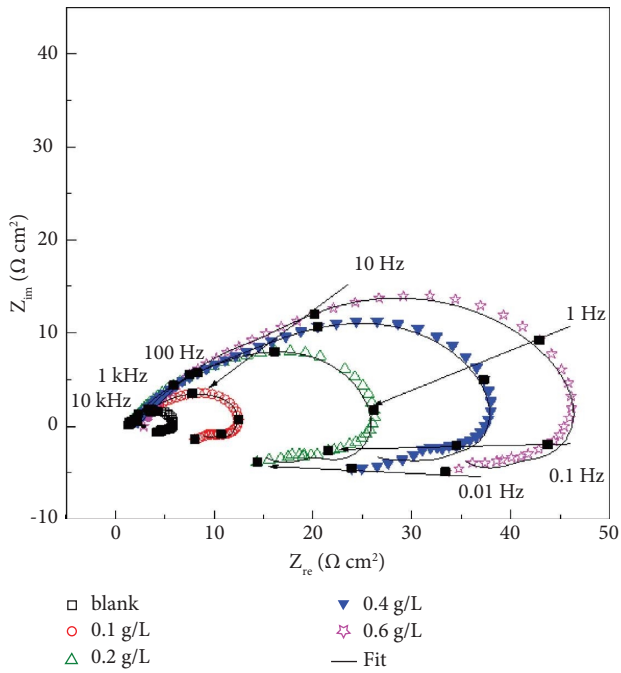

Figure 4: Nyquist plots of Al 2024 alloy in 1 M HCl in absence and presence of different concentrations of AHA extract at 298 K.

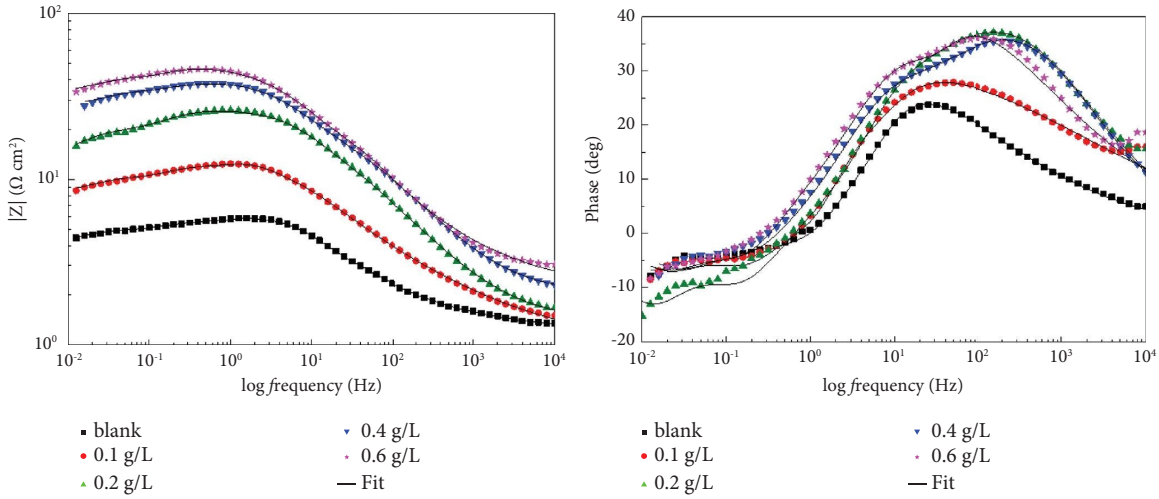

Figure 5: Bode plots of Al 2024 alloy in 1 M HCl in absence and presence of different concentrations of AHA extract at 298 K.

(Figure 5), it is observed that the Bode modulus at low frequency increases when the concentration of the AHA extract increases, indicating that the inhibitor is performing better. The Bode phase diagram of 2024 aluminum alloy without AHA extract shows three time constants, one at around 10^1 Hz for the oxide layer and two inductive loops at around 10^{-1}–10^{-2} Hz related to the relaxation of adsorbed species. The phase signal in the middle frequency range takes an asymmetrical shape in the presence of the inhibitor which suggests the overlapping of two time constants, one at around 10^1 Hz related to the oxide layer and the other at around 10^2 Hz related to the formation of the inhibitive film on the 2024 aluminum alloy surface. The phase angle of the two overlapped time constants increases with the AHAE concentration which can be related to an improved corrosion protection [43].

The time constants specific to the inhibitive layer are not clearly distinguished from the time constants related to the oxide film. Therefore, the experimental data were fitted with an electrical equivalent circuit with one capacitive loop in the high frequency range that comprises contributions from both the oxide layer and the inhibitive layer. The equivalent circuit used to analyze the data is shown in Figure 6. This model contains a solution resistance R_s, a parallel combination of a constant phase element CPE, a resistance R_1 and two inductive elements both constituted by a series combination of an inductance (L_1 and L_2) and an inductive resistance (R_{L1} and R_{L2}). This circuit has been widely used to

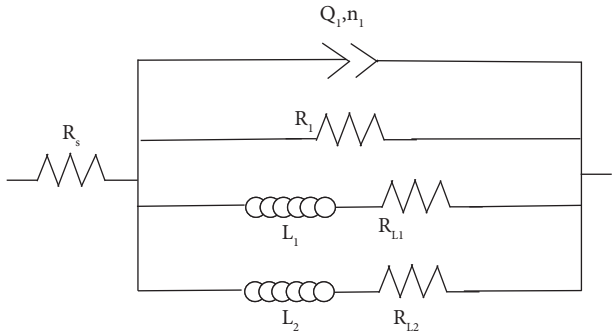

Figure 6: Electrical equivalent circuit used for the characterization of the Al 2024 alloy/solution interface in the absence and presence of AHA extract.

interpret the Al/HCl solution interface but in general with a single inductive time constant in the low-frequency part [29, 49, 50]. The appearance of two inductive loops was reported before for the corrosion of aluminium alloy AA3003 in HCl solution. [51].

The impedance parameters are given in Table 4. The χ^2 parameter was always below 5.10^{-2}. The impedance of CPE is given by

$$Z_{\mathrm{CPE}} = \left(Q_1 (j\omega)^{\mathrm{n}}\right)^{-1}, \tag{5}$$

where Q_1 is the magnitude of CPE and the exponent n has values between −1 and 1 with a value of 1 corresponding to a capacitor, a value of −1 characteristic of inductance and a value of 0.5 assigned to diffusion phenomena. The values of n are close to 0.5 which suggests that the interfacial reaction is under mass transport control by diffusion. A diffusional contribution to the high-frequency capacitive loop was also reported when dissolving Al in an acidic NaCl solution in the presence of 8-hydroxyquinoline. [52].

The polarization resistance R_p can be determined as the real part of impedance at the zero frequency limit. [45] The impedance associated with an inductor approaches zero as frequency approaches zero while that of a capacitor approaches infinity. Therefore, R_p can be calculated from the following equation:

$$R_p = \left(\frac{1}{R_1} + \frac{1}{R_{L1}} + \frac{1}{R_{L2}}\right)^{-1}. \tag{6}$$

The inhibitor efficiency (η_{EIS}) was calculated from R_p values using equation (3). A comparison of inhibitory efficiencies obtained using the a.c. and d.c. approaches reveal good agreement.

3.5. Adsorption Isotherm. The weight loss and electrochemical results showed that the inhibition efficiency increased with an increase in the concentration of the AHA extract. This fact suggests that the corrosion inhibition of the extract is due to the adsorption of AHA extract on the 2024 aluminum alloy surface. Different adsorption isotherm models (Langmuir, Frumkin, Freundlich, and Temkin models) [53] have been tested in order to get a better understanding of the interactions of the molecules of the extract with the 2024 aluminum alloy surface. Therefore, the surface coverage values, θ, calculated from the weight loss measurements at different concentrations of AHA extract, were used to demonstrate the adsorption isotherm model that best reflects the adsorption process of AHA extract on the 2024 aluminum alloy surface. The AHAE adsorption was best described by the Langmuir adsorption isotherm (Frumkin, Freundlich, and Temkin adsorption models are shown in SI, Figure S1). The Langmuir isotherm can be expressed by the following equation:

$$\frac{C}{\theta} = \frac{1}{K_{\mathrm{ads}}} + C, \tag{7}$$

where C is the inhibitor concentration, θ the degree of surface coverage and K_{ads} the equilibrium constant for adsorption process.

Figure 7 shows the plot of C/θ versus C, and a linear plot was obtained with a slope value close to unity and a linear regression coefficient (R^2) close to unity, indicating that the adsorption of inhibitor molecules on the 2024 aluminum alloy surface obeys the Langmuir isotherm. Equation (7) is generally associated with a Langmuir adsorption isotherm for a single component. The simplest theory for describing multicomponent adsorption equilibria is the extended Langmuir isotherm equation (54) considering a simple « one site » Langmuir competitive model (i.e., assuming one molecule per site and no lateral interactions), the total surface coverage is as follows:

$$\theta_T = \sum_{i=1}^{N} \theta_i = \frac{\sum_{i=1}^{N} k_i C_i}{1 + \sum_{i=1}^{N} k_i C_i}, \tag{8}$$

where N is the number of adsorbates in the natural extract and θ_i, k_i, and C_i stand for the fractional coverage, the adsorption equilibrium constant, and the concentration of the species i, respectively. The concentration C_i (in g/L) of each species i is related to the concentration of the extract C by

$$C_i = x_i C, \tag{9}$$

where x_i is the weight fraction of the species i in the extract.

Equation (8) could be rearranged into the equation as follows:

$$\frac{C}{\theta_T} = \frac{1}{\sum_{i=1}^{N} k_i x_i} + C. \tag{10}$$

According to equation (10), the plot of C/θ_T versus C gives a straight line with a slope = 1 and an intercept = $1/\sum_{i=1}^{N} k_i x_i$

Therefore, the experimental results obtained with the natural extract of artemisia are in agreement with the extended Langmuir isotherm equation adsorption model for multicomponent systems.

The K_{ads} value of AHA extract, obtained from the intercept of the Langmuir isotherm plot is ca. 27 $\mathrm{L{\cdot}g^{-1}}$. K_{ads} is related to the standard free energy of adsorption, $\Delta G^0_{\mathrm{ads}}$, as follows:

Table 4: Electrical parameters for AA2024 in 1M HCl in absence and in presence of different concentrations of AEAHA.

C_{AHA} (g/L)	R_s (Ω cm^2)	R_1 (Ω cm^2)	Q_1 (mΩ^{-1}s^{n}cm^{-2})	n_1	R_{L1} (Ω cm^2)	L_1 (H cm^2)	R_{L2} (Ω cm^2)	L_2 (H cm^2)	R_P (Ω cm^2)	η_{EIS} (%)
Blank	1.30	6.4	17.06	0.58	11.4	2.3	9.4	84.2	2.86	—
0.1	1.15	18.2	12.46	0.48	25.8	7.1	23.2	148.5	7.31	60.8
0.2	1.34	29.0	2.63	0.61	65.2	44.2	32.1	420.1	12.34	76.8
0.4	1.24	53.1	1.55	0.64	177.2	111.8	67.3	728.3	25.43	88.7
0.6	2.35	55.3	2.62	0.58	170.2	97.2	103.5	941.4	29.74	90.4

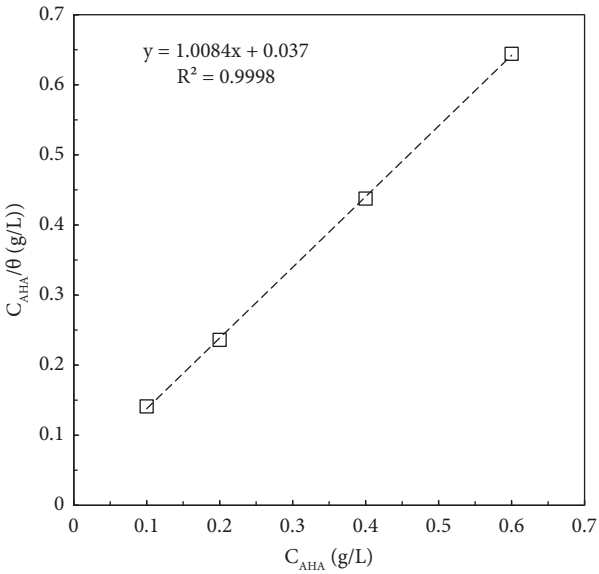

Figure 7: Langmuir's adsorption isotherm for AHA extract on Al 2024 alloy in 1 M HCl solution.

$$\Delta G^0_{ads} = -RT \quad \ln\left(K_{ads}\, C_{H_2O}\right), \tag{11}$$

where C_{H_2O} is the concentration of water in solution (in g/L), R the universal molar gas constant (8.314 J K^{-1} mol^{-1}), and T the temperature (298K). The calculated value of ΔG^0_{ads} was -25.3 kJ·mol^{-1}. The surface coverage values obtained from the other techniques also obey the Langmuir isotherm with linear correlation coefficients greater than 0.99 and giving ΔG^0_{ads} values of -23.5 kJ·mol^{-1}, -25.3 kJ·mol^{-1}, and -24.1 kJ·mol^{-1} from LPR, PPM and EIS methods, respectively. It is seen that the four methods used in the present work lead to fairly close values of the standard free energy of adsorption. The value of ΔG^0_{ads} is in the range of the values reported in the literature for plant extracts in HCl medium for aluminum which are between -3 and -38 kJ·mol^{-1} [26, 27, 29, 55]. The negative value of ΔG^0_{ads} shows that the adsorption of inhibitor molecules from AHA extract on the 2024 aluminum alloy surface is a spontaneous process. It is generally established that ΔG^0_{ads} values around -20 kJ·mol^{-1} or lower indicate a physical adsorption, while those of -40 kJ·mol^{-1} or higher involves a chemical adsorption and charge sharing or a transfer from the inhibitor molecules to the metal surface to form a coordinate type of bond [56]. As recently discussed in depth by Kokalj et al. [57], this criterion of 20/40 is questionable for several reasons: the enthalpy of adsorption is more representative of the forces of adsorption bonds, physisorption may be strong due to a multisite adsorption for the same molecule and bond-breaking or large adsorbate distortions during chemisorption can result in a rather weak standard free energy of adsorption. [57] The negative value of ΔG^0_{ads} demonstrates that the adsorption process is spontaneous and we showed that the values of ΔG^0_{ads} obtained are in the range of the values reported in the literature with other natural extracts. However, it is not possible to reliably determine the mode of adsorption simply from the value of the free energy of adsorption. On the other hand, it is important to note that the standard free energy of adsorption was determined from equation (11) considering the concentrations in g/L (water and extract). This is obviously linked to the lack of knowledge of the active molecules of the natural extract and their real concentration in the extract. Although it has been used by many authors [58–60], this method is not satisfactory for extracting the actual thermodynamic parameters (free energy, enthalpy, and entropy of adsorption) because adsorption equilibrium is based on molecular exchange and not mass exchange. This limitation has been noted by other authors [61, 62]. The discussion added in supporting information leads to the conclusion that the actual free energy of adsorption is certainly more negative than the value calculated from mass concentrations of the aqueous extract of AHA (-25.3 kJ·mol^{-1}).

3.6. Effect of Temperature. In order to study the effect of temperature on the corrosion reaction, gravimetric monitoring was carried out at a temperature range of 298–328 K both in the absence and in the presence of the optimal concentration of the AHA extract (0.6 g/L). The effect of temperature on corrosion rate and inhibition efficiency is shown in Figure 8. The corrosion rate increases with temperature in both the blank and inhibited solutions. It is also seen that the percent protection decreases with the rise in temperature. This probably reflects the desorption or decomposition of the active molecules of the extract when the temperature increases. This is possibly related to the high rate of dissolution and hydrogen production at high temperature which could hinder the adsorption of the inhibitor on the surface. The apparent activation energy (E_a) for the corrosion reaction was calculated from an Arrhenius-type plot according to the following equation:

$$\text{Ln CR} = \text{Ln}\, A - \frac{E_a}{RT}, \tag{12}$$

where A is the pre-exponential factor, T the temperature (K), and R the universal molar gas constant.

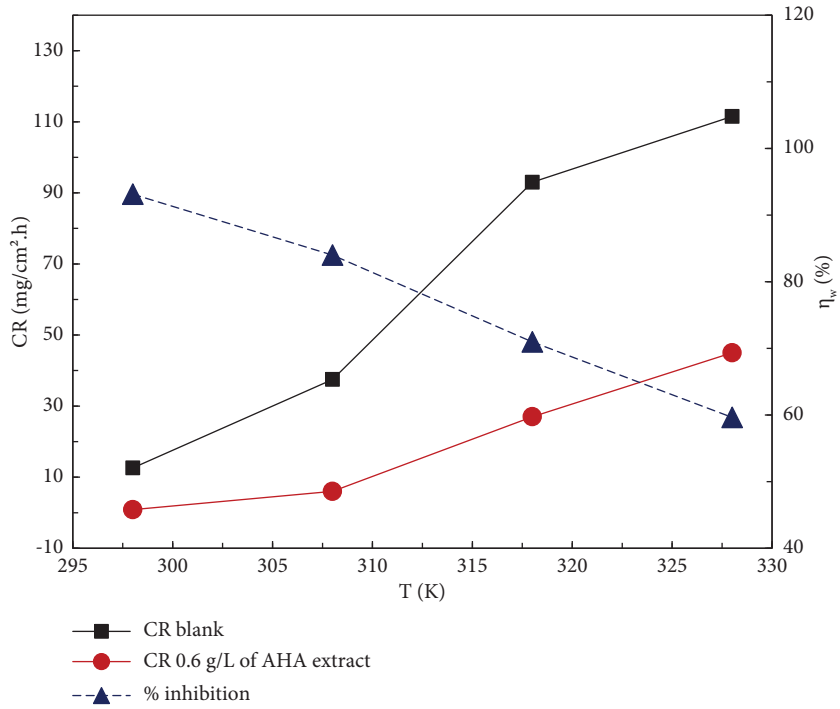

Figure 8: Corrosion rate and inhibition efficiency at various temperatures for Al 2024 alloy corrosion in 1 M HCl in the absence and presence of AHA extract at optimal concentration 0.6 g/L.

Figure 9 displays the Arrhenius plots in the absence and presence of 0.6 g/L of AHA extract. The temperature has a more marked effect on the rate of corrosion in the presence than in the absence of the extract. A higher E_a value in the inhibited corrosion solution is often interpreted as physisorption [63, 64]. On the other hand, chemisorption is generally associated to higher E_a values for free acid solutions compared to the inhibited one. The temperature effect on the inhibited corrosion reaction is very complex. Riggs and Hurd [65] showed that a decrease in activation energy value arises at a high level of coverage (>0.95) from the shift of a net corrosion reaction from that on the free surface to one involving the adsorbed sites directly. It must however be noted that the activation energy involved in the adsorbed species can be either larger or smaller from that involved in the simple metal/acid reaction. It is also noted that a decrease in E_a value can also occur at low coverages when adsorption process is endothermic, which is necessarily associated to chemisorption [66]. The E_a values for the corrosion in the absence and presence of AHA extract were 61 kJ·mol^{-1} and 109 kJ·mol^{-1}, respectively. The larger E_a value in presence of the AHA extract can be interpreted as physisorption. It also suggests that the net corrosion rate is controlled by the corrosion rate in the uncovered area ie that the extent of adsorption is rate-determining [65]. In that case, the activation energy increases with the surface coverage (when adsorption is exothermic) to approach the maximal value $E_1 + Q$ at high coverage with E_1 the activation energy of the unhibited (blank) solution and Q the heat of adsorption (=$-\Delta H_{ads}$).

According to the thermodynamic basic equation, $\Delta G^0_{ads} = \Delta H^0_{ads} - T\Delta S^0_{ads}$, the Langmuir adsorption isotherm can be rearranged to give

$$\mathrm{Ln}\frac{\theta}{1-\theta} = \mathrm{Ln}\frac{C}{C_{H2O}} + \frac{\Delta S^0_{ads}}{R} - \frac{\Delta H^0_{ads}}{\mathrm{RT}}. \quad (13)$$

An estimate of the standard adsorption enthalpy (ΔH^0_{ads}) and adsorption entropy (ΔS^0_{ads}) can be deduced from equation (13). Figure 10 shows the plot of Ln(θ/(1 − θ)) versus 1/T which gives a straight line with slope of $\Delta H^0_{ads}/R$ and intercept of ($\Delta S^o_{ads}/R$ + Ln (C/C_{H2O})). The calculated ΔH^0_{ads} is −60.5 kJ·mol^{-1} and the ΔS^0_{ads} value is −120.5 J·mol^{-1}·K^{-1}. The negative value of ΔH^0_{ads} indicates that the adsorption of the molecules of AHA extract on the Al alloy is exothermic. It is noted that the calculated Ea value in the inhibited solution (109 kJ·mol^{-1}) is numerically close to the maximal value E_1 + Q (121 kJ·mol^{-1}). This is consistent with the fairly high coverage expected at the optimal concentration of the AHA extract (0.6 g/L).

3.7. Morphological Observations. The effect of AHA extract on corrosion process of 2024 aluminum alloy in 1M HCl was examined by the SEM micrographs of Al surfaces in the absence and presence of AHA extract as seen in Figure 11.

The SEM image of the freshly polished 2024 aluminum alloy surface revealed intermetallic particles IMPs of different sizes that can be classified according to their composition determined by EDX analysis (Figure 11(a)). Fe-rich particles including the Al-Cu-Fe-Mn and Al-Cu-Fe-Mn-Si

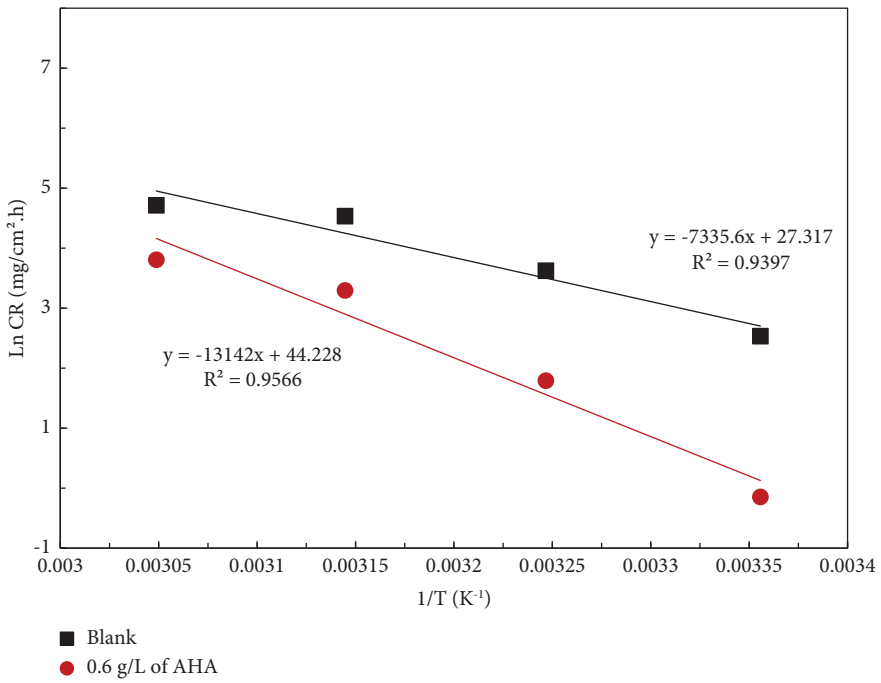

Figure 9: Arrhenius plots for Al 2024 alloy in 1M HCl in the absence and presence of AHA extract at 0.6 g/L.

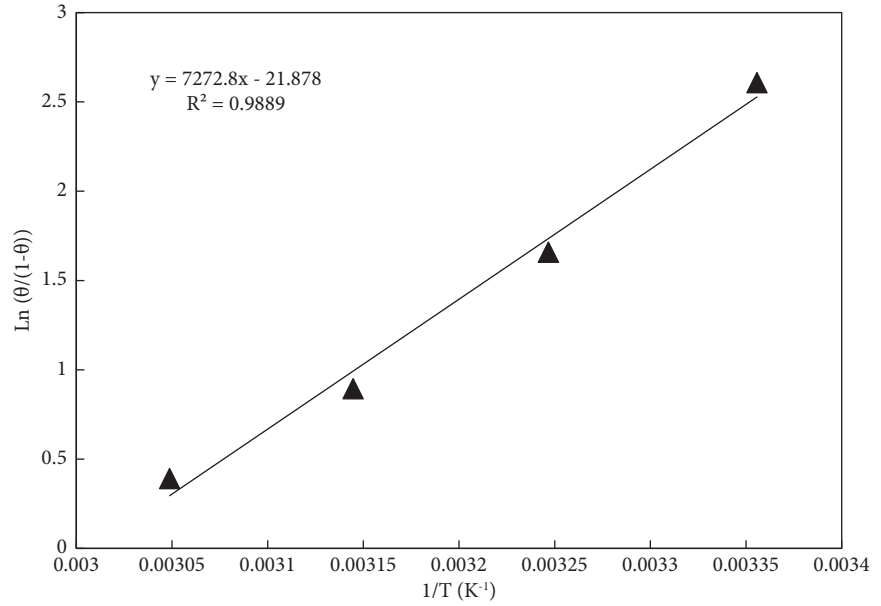

Figure 10: Plot of Ln $(\theta/1-\theta)$ at a concentration of AHA extract of 0.6 g/L against 1/T.

phases [67] have been identified in addition to IMPs associated with the magnesium-rich S phase (Al_2CuMg particles). The latter are more spherical in shape and smaller in size (<10 μm) than the former. After 1 h of immersion in 1M HCl, the 2024 aluminum alloy surface appears severely damaged as shown in Figure 11(b). The presence of several holes of different sizes shows that many IMPs were completely etched out after exposure to the corrosive environment.

The disappearance of the polishing scratches also shows that the corrosion is not only due to the trenching of cathodic IMPs or dissolution of the anodic IMPs but that uniform corrosion also occurs on the 2024 aluminum alloy surface in 1M HCl. After immersion in the corrosive solution containing 0.4 g/L of AHA extract, the surface appears much less damaged but a few holes are still identified on the SEM image in Figure 11(c). Although few holes can be still observed, the 2024 aluminum alloy surface appears even less degraded with the optimum concentration (0.6 g/L) of AHA extract (Figure 11(d)). The low degree of degradation of the alloy surface in the presence of the inhibitor extract in the HCl medium is confirmed by the polishing scratches still visible on the SEM images.

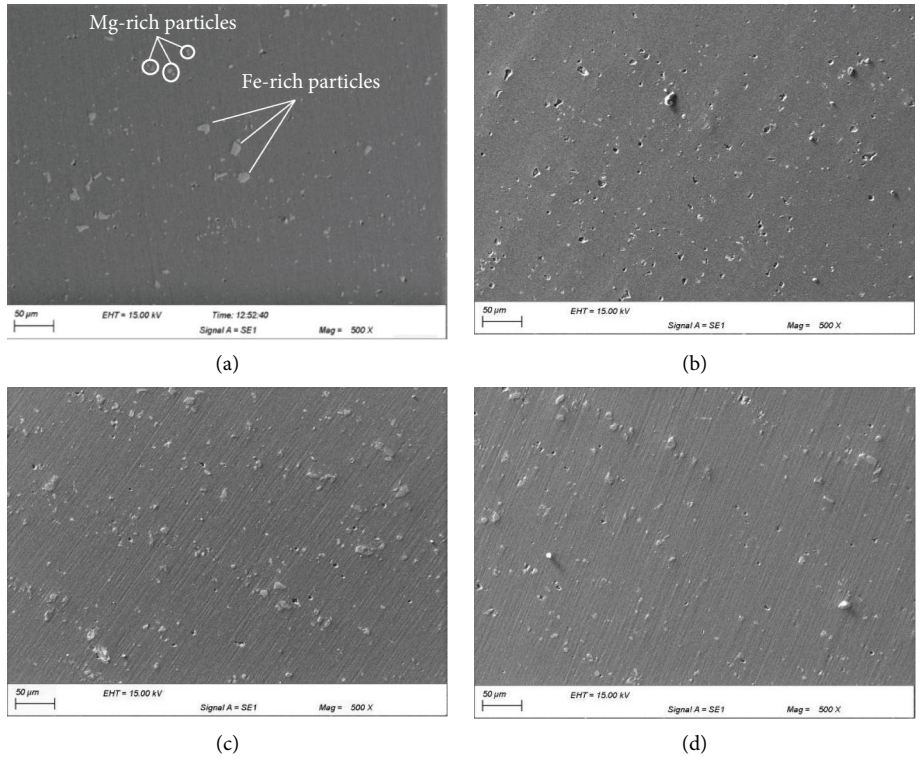

Figure 11: SEM micrographs of Al 2024 alloy surfaces (a) before immersion and after 1 h of immersion in (b) 1M HCl, (c) 1M HCl + 0.4 g/L AHA extract and (d) 1M HCl + 0.6 g/L AHA extract.

Therefore, the SEM images show that the dissolution of aluminum in 1M HCl was strongly reduced in the presence of the AHA extract.

3.8. Corrosion Inhibitor Active Components of AHAE. There has been extensive research on the composition of the essential oil of AHA [68, 69] but few studies relate to the analysis of the composition of its aqueous extracts [31]. The chemical profile of AHA extracts is subject to many variables, such as the harvest period or the geographical area [70]. Therefore, the analysis of the composition of the extract is required in order to determine which chemical compounds are linked to the inhibitory activity. The phytochemical LC-MS/MS based analysis of AHAE allowed the detection of more than 80 compounds (Table S1). Most of these compounds were sesquiterpenoids which agrees with previous works dealing with this species describing the presence of numerous sesquiterpene lactones [71]. Other terpenes, such as monoterpenes and diterpenes, were also detected while several flavonoids (putatively annotated as vicenin-2, schaftoside, isoschaftoside, isovitexin, hispidulin, and jaceosidin) were also included in the composition of AHAE [30, 72]. Other molecules were also identified such as aminoacids (valine and leucine), nicotinic acid, pyrimidine derivatives (thymine), 4-hydroxyacetophenone, and coumarin derivatives (scopoletin, fraxidin, isofraxidin, and esculetin). No quinic acid derivatives were detected in the present study, highlighting the variability in the composition of AHA extracts. It is indeed well known that the composition of natural extract is subject to great variability depending on the origin and age of the plant, the harvesting season, the growth stage, the variability of plant parts, and the extraction procedure (deterioration of active components). The AHAE is particularly rich in sesquiterpenes and flavonoids. Figure 12 shows the chemical structure of the main constituent for each subclass of metabolite in the extract: valine (Val), deoxyartemisin (Deox), isoschaftoside (Isos), and isofraxidin (Isof). The other constituents are either present in small proportions or belong to the same class of metabolite and therefore have a similar chemical structure. Val, Deox, Isos, and Isof contain heteroatoms (O and N), π-electron centers and aromatic rings. These electron-rich structures are likely to adsorb strongly on the surface of metals. Valine was reported to inhibit the corrosion of Al in an acidic solution but less efficiently than amino acids with sulfur atom or aromatic groups [73]. On the other hand, coumarin is a mixed-type inhibitor for Al in a neutral chloride solution [74], artemisinin has been already reported to be a good inhibitor of mild steel in an H_2SO_4 solution [75], and flavonoids are phenolic derivatives containing polar groups that enhance the adsorption on the metal surface [76]. Val, Deox, Isof, and Isos are therefore potential inhibitors, and dft analyses were conducted to evaluate and compare the types of interactions and their ability to adsorb to the metal surface. First, the spatial molecular structure and molecular electronic structure of the main components of the extract based on quantum chemical calculations both provide indications of how these molecules would adsorb. From the geometrical point of

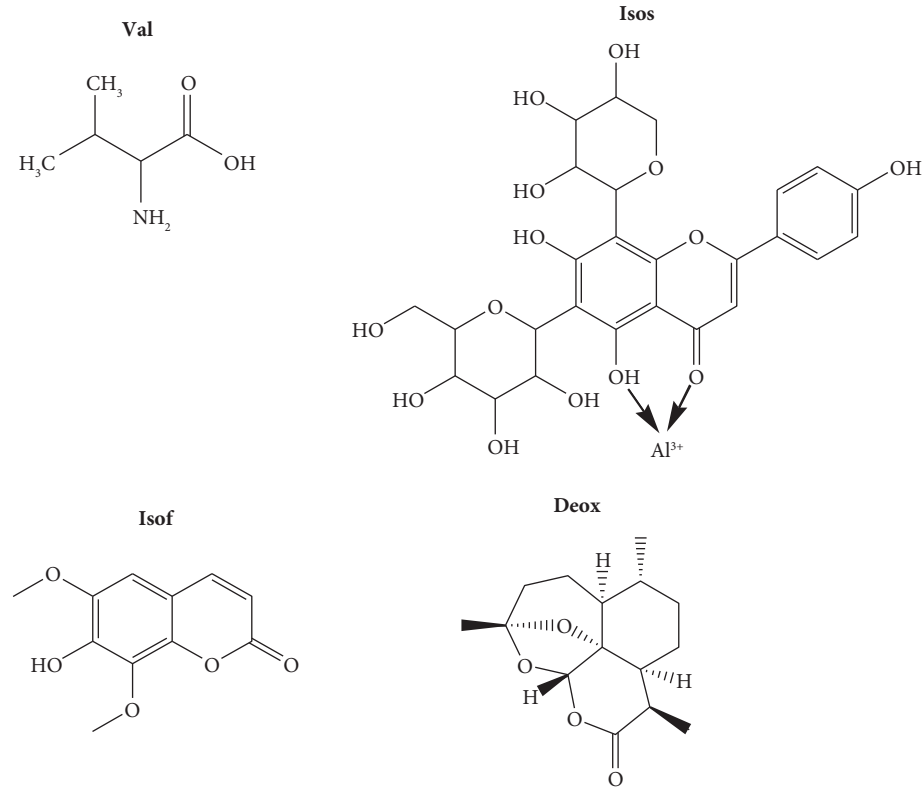

Figure 12: Molecular structure of the principal components of AEAHA: valine (amino acid), Val, isoschaftoside (flavonoid), Isos, isofraxidin (coumarine), Isof and deoxyartemisinin (sesquiterpene), Deox. Possible chelating site for Al(III)-Isos complexes.

view, it can be seen from Figure 13 that, in contrast to Deox and Val, Isof molecule is planar, and Isos is almost planar. Isof and Isos have π-conjugated systems that make the electrons delocalization very easy. From the electronic structure point of view, all the studied molecules have several oxygen atoms that are known for their electro-attractor effect. Oxygen and nitrogen atoms, because they are more electronegative than *C* and *H*, would be the centers of concentration of negative charges. This is precisely what the electronic density images of Figure 13 show. The high electronic density is localized around the carbonyl, more precisely on the oxygen. Two different ways of electronic density distribution schemes can be distinguished for these four molecules: localized in the case of Val and Deox and delocalized in Isof and Isos.

In the frontier molecular orbitals (FMO) theory, the reactivity of a molecule is described by the energy and the shape of the frontier molecular orbitals: the highest occupied molecular orbital (HOMO) and the lowest unoccupied molecular orbital (LUMO). The HOMO is related to the ability of a molecule to donate electrons; the LUMO provides information on the ability of a molecule to accept electrons. Alongside the electronic density study, the FMO approach is of prime importance. In fact, in addition to informing us about the preferential sites for electrophilic or nucleophilic attacks, these orbitals show the direction of an attack. The frontier molecular orbitals of the four studied molecules are given in Figure 14. In the case of Isof, Deox, and Isos there are many molecular orbitals whose energies are equivalent to that of HOMO; these are the double bonds and the oxygen lone pairs. From Figure 14, it is seen that the HOMO and LUMO of Val and Deox are both localized on the oxygen of carbonyl while the HOMO and LUMO in Isof and Isos have different locations. The HOMO location of Isof is the O lone pair of the C=O which corresponds to the same adsorption site identified by Tan et al. [74] with coumarin. The E_{HOMO} values for the four structures tested are almost the same which suggests a comparable tendency to donate electrons to the metal surface through its HOMO. On the other hand, the E_{LUMO} values vary much more significantly in the order Isos < Isof < Deox < val. This result indicates that surface to molecule backdonation of electrons is favored in the case of Isos and Isof in connection with the low E_{LUMO} values of these molecules. This agrees with the results of Tan et al. which showed that electron donation occurred from the aluminum surface to coumarin (with a structure close to Isof). [74] In comparison, Val and Deox can donate electrons to the Al surface but cannot receive donated electrons from the Al surface in return. The donation of electrons from the HOMO and the backdonation of electrons from the metal to the LUMO can be beneficial for a high inhibition efficiency of Isos and Isof. The electronegativity χ represents the ability of the molecule to attract electrons. Table 5 shows that Isos has the highest electronegativity among the studied molecules; therefore, it has the highest ability to accept electrons from the metal surface, which agrees with the E_{LUMO} trend. The dipole moment of the molecules evolves in the direction Isof > Isos > Deox > Val. High-dipole moment

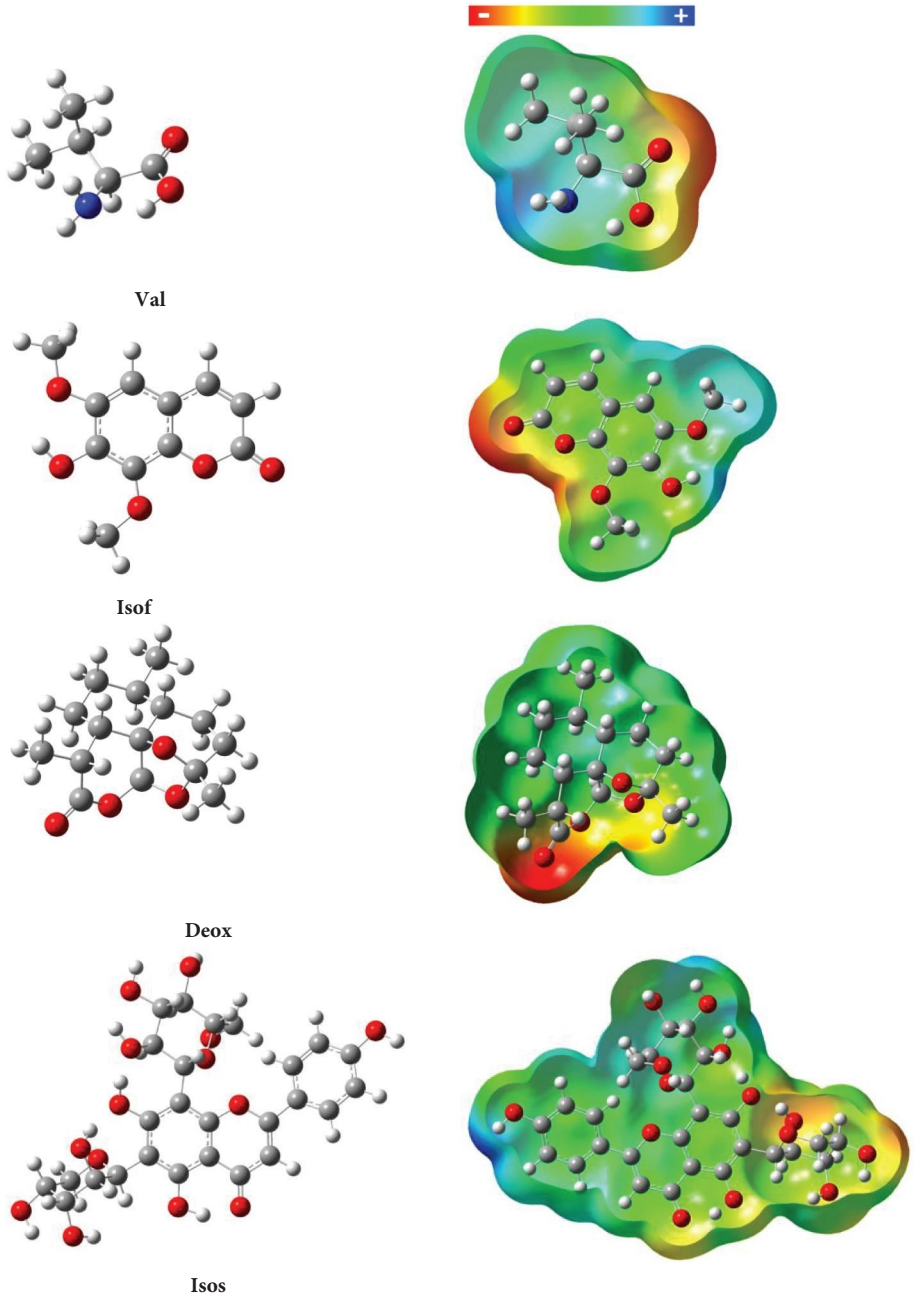

Figure 13: The optimized geometrical and electrostatic potential structures of Val, Isof, Deox and Isos using DFT/B3LYP/6-31þ þG(d, p).

molecules tend to form strong dipole-dipole interactions with the metal thus enhancing their adsorption. However, a high dipole moment does not necessarily go with a high degree of inhibition because it can also lead to repulsive lateral interactions between the adsorbed molecules. [77].

The chemical hardness is closely related to the HOMO-LUMO energy gap ($\eta = \Delta E/2$) and it designates the resistance of a molecule to any deformation of its electronic cloud. From the HSAB principle, soft acids prefer to combine with soft bases. Metal atoms are known as soft acids. Note that the presence of chloride ions in the corrosive medium can increase the softness of metal, as shown by Aramaki et al. [78]. These authors showed that the inhibition of a soft base increased with the concentration of HCl in a $HClO_4$-HCl solution. The soft base inhibitor is easily adsorbed on the surface where chloride adsorbs because the adsorption of chloride increases the softness of a metal as an acid. Thus, soft–soft interaction is the most predominant factor for the adsorption of inhibitor molecules. It is seen from Table 5 that the values of softness (the inverse of global hardness, η) follow the order Isos > Isof > Deox > Val, which further supports the better adsorption ability of Isos and Isof on the metal surface.

In addition to the inhibitor-metal interactions, the formation of Al^{3+}-inhibitor complexes on the surface must also be taken into account according to the HSAB principle.

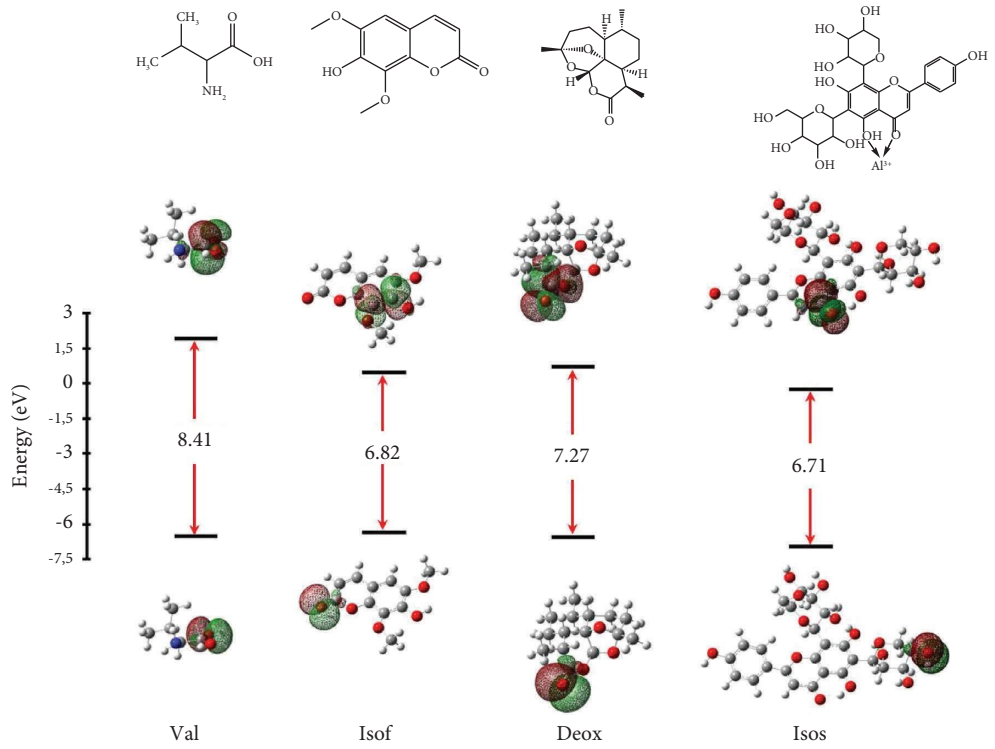

Figure 14: Frontier molecular orbitals HOMO and LUMO of the four studied molecules.

Table 5: Rectivity descriptors of the four extract components.

	μ (D)	E_{HOMO} (eV)	E_{LUMO} (eV)	χ (eV)	η (eV)
Val	5.189	−6.51	1.90	2.31	4.20
Isof	7.760	−6.34	0.47	2.94	3.41
Deox	5.456	−6.56	0.71	2.92	3.63
Isos	13.683	−6.96	−0.26	3.61	3.35

Small and highly charged Al^{3+} cations are hard acids that will tend to form complexes with ligands with hard N and O atoms. Val, Deox, Isos, and Isof all contain O and/or N groups and therefore can bind with Al^{3+} ions. This agrees well with previous results showing the formation of Al-coumarin [74] at the metal surface exposed to a chloride solution. Besides, flavonoids coordinate Al ions in their neutral form (their form in acidic conditions) via the α-hydroxycarbonyl site (Figure 12) [79]. Since Al^{3+} cations are produced on the anodic sites, the Al(III)-Isof and Al(III)-Isos complexes are likely to form preferentially on or near these anodic sites and thus reduce the dissolution of the aluminium. This is consistent with the mixed character of the inhibition, indicating a partial inhibition of the anodic reactions.

The adsorption bonding trends of the active molecules of AHA extract is summarized in Figure 15.

Figure 15 shows the most active molecules of the extract (isoschaftoside and isofraxidin) inhibiting both cathodic and anodic reactions by adsorbing to the surface and by forming chelate complexes with Al^{3+} ions. The preferential donation and backdonation sites also shown in the figure are derived from molecular modelling. It is also shown that chelate formation certainly occurs mainly near the sites that generate Al^{3+} cations, i.e., the anode sites. Different kinds of intermetallic particles were found in the structure of AA2024, the main ones being the S-phase with Al_2CuMg composition and the Al_6 (Cu, Fe, Mn) intermetallics [80]. All kinds of intermetallics excepting S-phase are composed of metals nobler than aluminum, thus showing cathodic character. The S phase is first dissolved at the first stage of pitting corrosion in Cl^- media. However, after selective dissolution of Mg and Al, the porous Cu remnants become cathodic with respect to the Al matrix [80]. This copper enrichment of the surface is in line with the observed evolution of OCP (Figure 1). For the sake of simplicity, intermetallic particles are considered cathodic in Figure 15, even though some of these compounds may be at least temporarily anodic. The fact that the extract molecules inhibit the cathodic reaction more strongly than the anodic reaction (as revealed by potentiodynamic measurements) suggests that they are strongly adsorbed on these cathodic sites.

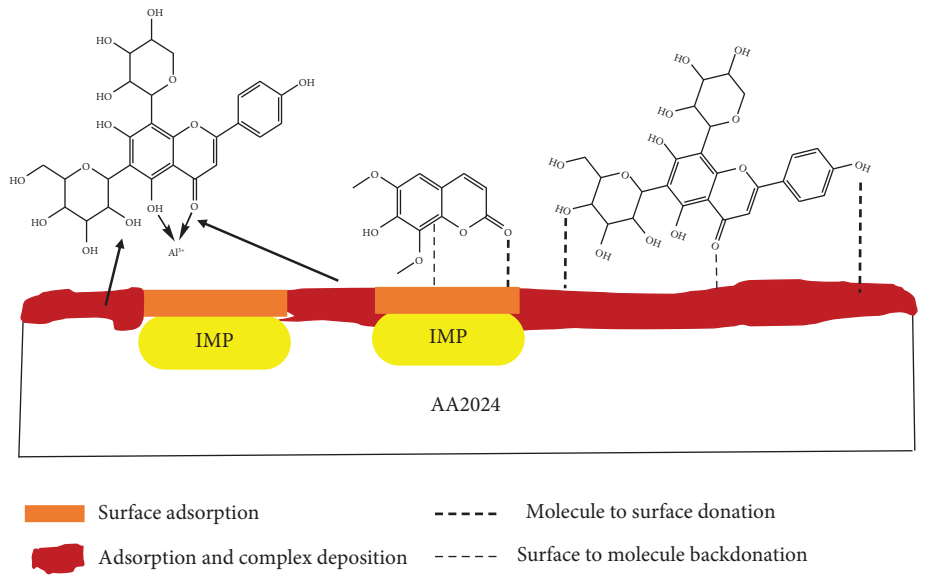

Figure 15: Schematic illustration of the adsorption bonding trends of the main active molecules of AHA aqueous extract on 2024-T3 aluminum alloy surface.

4. Conclusions

The corrosion inhibition capability of AHAE for preventing corrosion of 2024 aluminum alloy in 1M HCl can be summarized by the following conclusions:

(1) The molecules of the extract act as mixed inhibitors but inhibit the cathodic reaction more efficiently.

(2) The inhibition of corrosion took place by the adsorption of the molecules of the extract on the Al surface. The results showed that the adsorbed molecules do not simply act by physically blocking the cathodic sites but also affect the mechanism of the hydrogen evolution reaction.

(3) Adsorption isotherms in multicomponent systems such as natural extracts can be extremely complex from a mathematical point of view. Herein, the adsorption of the natural extract follows the extended Langmuir isotherm equation adsorption model for multicomponent systems which is the simplest theory for describing multicomponent adsorption equilibria.

(4) SEM images showed that the AHAE reduced the localized corrosion activity related to intermetallic particles as well as the Al matrix dissolution.

(5) Weight loss measurements have been carried out in the temperature range 25–55°C to obtain more information about the main mode of adsorption of the active molecules of the extract. The results showed a decrease in the effectiveness of the inhibitor and an increase in the activation energy of the corrosion reaction in the presence of the aqueous extract which can be interpreted as physisorption.

(6) Following LC-MS/MS analysis, four main molecules representative of the different metabolites of the extract and with potential inhibitor activity were identified: valine, isofraxidin, deoxyartemisin, and isoschaftoside.

(7) The quantum chemical calculations revealed that isoschaftoside and isofraxidin have a higher ability to accept electrons from the metal than valine and deoxyarmetisinin. The surface-to-molecule back-donation is an important interaction as it can reinforce the adsorption of the molecule on the aluminum surface. Moreover, isofraxidin and isoschaftoside easily form complexes with aluminium ions which could contribute to the high inhibition efficiency of the extract.

(8) This study demonstrated the high efficiency of aqueous Artemisia extracts in inhibiting corrosion of 2024 aluminum alloy in acidic solutions at moderate temperatures such as those encountered during pickling operations.

Data Availability

The data that support the findings of this study are available from the corresponding author upon reasonable request.

Conflicts of Interest

The authors declare that there are no conflicts of interest.

Acknowledgments

We acknowledge Dr Kamilia Ould Lamara at Tizi Ouzou university, Algeria for carrying out the SEM analyzes and Pr Sarri Djamel at the University of Msila, Algeria for the identification of the plant. The financial support from the Ministry of Higher Education & Scientific Research of Algeria and France is gratefully acknowledged (Profas B+ scholarship). The authors wish to thank Dr S. Greff

(Aix-Marseille University, IMBE, France) for the LC-MS/MS experiments which were conducted on the regional metabolomics platform MALLABAR. Open Access funding enabled and organized by COUPERIN CY23.

Supplementary Materials

Temkin, Freundlich, and Frunmkin adsorption isotherms are shown in supplementary file as Figure S1. A critical discussion about the actual free energy of adsorption for natural extracts is also acarried out and chemical compounds detected by LC-MS/MS are given in Table S1. (*Supplementary Materials*)

References

[1] L. F. Mondolfo, *Aluminum Alloys: Structure and Properties*, Elsevier Science, Kent, Non-Metropolitan, 2013.

[2] C. Vargel, *Corrosion of Aluminium*, Elsevier B.V, Amsterdam, The Netherlands, 2004.

[3] M. Pourbaix, *Atlas of Electrochemical Equilibria in Aqueous Solutions*, Pergamon Press, Oxford, UK, 1966.

[4] D. M. Dražić, S. K. Zečević, R. T. Atanasoski, and A. R. Despić, "The effect of anions on the electrochemical behaviour of aluminium," *Electrochimica Acta*, vol. 28, no. 5, pp. 751–755, 1983.

[5] F. D. Bogar and R. T. Foley, "The influence of chloride ion on the pitting of aluminum," *Journal of the Electrochemical Society*, vol. 119, no. 4, p. 462, 1972.

[6] P. L. Cabot, F. A. Centellas, J. A. Garrido, E. Pérez, and H. Vidal, "Electrochemical study of aluminium corrosion in acid chloride solutions," *Electrochimica Acta*, vol. 36, no. 1, pp. 179–187, 1991.

[7] S. M. Garcia, "Aluminum cleaning and brightening composition and method of manufacture thereof," US4970014A, 1990.

[8] R. Xiao, K. Yan, J. Yan, and J. Wang, "Electrochemical etching model in aluminum foil for capacitor," *Corrosion Science*, vol. 50, no. 6, pp. 1576–1583, 2008.

[9] C. Ban, Y. He, X. Shao, and Z. Wang, "Effects of polymer corrosion inhibitor on widening etch tunnels of aluminum foil for capacitor," *Corrosion Science*, vol. 78, pp. 7–12, 2014.

[10] I. L. Rosenfeld and I. K. Marshakov, "Mechanism of crevice corrosion," *Corrosion*, vol. 20, no. 4, pp. 115t–125t, 2013.

[11] S. Z. Salleh, A. H. Yusoff, S. K. Zakaria et al., "Plant extracts as green corrosion inhibitor for ferrous metal alloys: a review," *Journal of Cleaner Production*, vol. 304, Article ID 127030, 2021.

[12] A. Zakeri, E. Bahmani, and A. S. R. Aghdam, "Plant extracts as sustainable and green corrosion inhibitors for protection of ferrous metals in corrosive media: a mini review," *Corrosion Communications*, vol. 5, pp. 25–38, 2022.

[13] C. Verma, E. E. Ebenso, I. Bahadur, and M. A. Quraishi, "An overview on plant extracts as environmental sustainable and green corrosion inhibitors for metals and alloys in aggressive corrosive media," *Journal of Molecular Liquids*, vol. 266, pp. 577–590, 2018.

[14] N. Chaubey, Savita, A. Qurashi, D. S. Chauhan, and M. A. Quraishi, "Frontiers and advances in green and sustainable inhibitors for corrosion applications: a critical review," *Journal of Molecular Liquids*, vol. 321, Article ID 114385, 2021.

[15] S. A. Umoren, M. M. Solomon, I. B. Obot, and R. K. Suleiman, "A critical review on the recent studies on plant biomaterials as corrosion inhibitors for industrial metals," *Journal of Industrial and Engineering Chemistry*, vol. 76, pp. 91–115, 2019.

[16] A. Thakur and A. Kumar, "Sustainable inhibitors for corrosion mitigation in aggressive corrosive media: a comprehensive study," *Journal of Bio-and Tribo-Corrosion*, vol. 7, no. 2, p. 67, 2021.

[17] I. B. Obot and N. O. Obi-Egbedi, "An interesting and efficient green corrosion inhibitor for aluminium from extracts of Chlomolaena odorata L. in acidic solution," *Journal of Applied Electrochemistry*, vol. 40, no. 11, pp. 1977–1984, 2010.

[18] D. G. Ladha, N. K. Shah, Z. Ghelichkhah et al., "Experimental and computational evaluation of illicium verum as a novel eco-friendly corrosion inhibitor for aluminium," *Materials and Corrosion*, vol. 69, no. 1, pp. 125–139, 2018.

[19] S. R. S. Rodrigues, V. Dalmoro, and J. H. Z. dos Santos, "An evaluation of *Acacia mearnsii* tannin as an aluminum corrosion inhibitor in acid, alkaline, and neutral media," *Materials and Corrosion*, vol. 71, no. 7, pp. 1160–1174, 2020.

[20] L. A. L. Guedes, K. G. Bacca, N. F. Lopes, and E. M. da Costa, "Tannin of *Acacia mearnsii* as green corrosion inhibitor for AA7075-T6 alluminum alloy in acidic medium," *Materials and Corrosion*, vol. 70, no. 7, pp. 1288–1297, 2019.

[21] H. Gerengi, "Anticorrosive properties of date palm (*Phoenix dactylifera* L.) fruit juice on 7075 type aluminum alloy in 3.5% NaCl solution," *Industrial and Engineering Chemistry Research*, vol. 51, no. 39, pp. 12835–12843, 2012.

[22] S. A. Umoren, I. B. Obot, L. E. Akpabio, and S. E. Etuk, "Adsorption and corrosive inhibitive properties of*Vigna unguiculata*in alkaline and acidic media," *Pigment and Resin Technology*, vol. 37, no. 2, pp. 98–105, 2008.

[23] A. Singh, Y. Lin, W. Liu et al., "Plant derived cationic dye as an effective corrosion inhibitor for 7075 aluminum alloy in 3.5% NaCl solution," *Journal of Industrial and Engineering Chemistry*, vol. 20, no. 6, pp. 4276–4285, 2014.

[24] P. O. Ameh and N. O. Eddy, "Commiphora pedunculata gum as a green inhibitor for the corrosion of aluminium alloy in 0.1 M HCl," *Research on Chemical Intermediates*, vol. 40, no. 8, pp. 2641–2649, 2014.

[25] A. Khadraoui, A. Khelifa, K. Hachama, and R. Mehdaoui, "Thymus algeriensis extract as a new eco-friendly corrosion inhibitor for 2024 aluminium alloy in 1M HCl medium," *Journal of Molecular Liquids*, vol. 214, pp. 293–297, 2016.

[26] S. A. Umoren, I. B. Obot, E. E. Ebenso, and N. O. Obi-Egbedi, "The Inhibition of aluminium corrosion in hydrochloric acid solution by exudate gum from Raphia hookeri," *Desalination*, vol. 247, no. 1-3, pp. 561–572, 2009.

[27] A. Y. El-Etre, "Inhibition of aluminum corrosion using Opuntia extract," *Corrosion Science*, vol. 45, no. 11, pp. 2485–2495, 2003.

[28] E. E. Oguzie, "Corrosion inhibition of aluminium in acidic and alkaline media by Sansevieria trifasciata extract," *Corrosion Science*, vol. 49, no. 3, pp. 1527–1539, 2007.

[29] S. Deng and X. Li, "Inhibition by Jasminum nudiflorum Lindl. leaves extract of the corrosion of aluminium in HCl solution," *Corrosion Science*, vol. 64, pp. 253–262, 2012.

[30] S. Bourgou, I. Bettaieb Rebey, K. Mkadmini, H. Isoda, R. Ksouri, and W. M. Ksouri, "LC-ESI-TOF-MS and GC-MS profiling of Artemisia herba-alba and evaluation of its bioactive properties," *Food Research International*, vol. 99, pp. 702–712, 2017.

[31] A. I. Arroyo, Y. Pueyo, F. Pellissier et al., "Phytotoxic effects of volatile and water soluble chemicals of Artemisia herba-alba," *Journal of Arid Environments*, vol. 151, pp. 1–8, 2018.

[32] A. M. Esmail, A. E.-H. H. Mohamed, M. A. El-Sayed, M. E. Hegazy, S. E. Helaly, and N. S. Mohamed, "Chemical constituents and biological activities of Artemisia herba-alba," 2015, https://www.researchgate.net/publication/280528273_Chemical_constituents_and_biological_activities_of_Artemisia_herba-alba.

[33] F. Younsi, N. Rahali, S. Mehdi, M. Boussaid, and C. Messaoud, "Relationship between chemotypic and genetic diversity of natural populations of Artemisia herba-alba Asso growing wild in Tunisia," *Phytochemistry*, vol. 148, pp. 48–56, 2018.

[34] M. Benabdellah, M. Benkaddour, B. Hammouti, M. Bendahhou, and A. Aouniti, "Inhibition of steel corrosion in 2M H3PO4 by artemisia oil," *Applied Surface Science*, vol. 252, no. 18, pp. 6212–6217, 2006.

[35] M. Boudalia, R. M. Fernández-Domene, M. Tabyaoui, A. Bellaouchou, A. Guenbour, and J. García-Antón, "Green approach to corrosion inhibition of stainless steel in phosphoric acid of Artemesia herba albamedium using plant extract," *Journal of Materials Research and Technology*, vol. 8, no. 6, pp. 5763–5773, 2019.

[36] O. Ouachikh, A. Bouyanzer, M. Bouklah et al., "Application of essential oil of *artemisia herba alba* as green corrosion inhibitor for steel in 0.5 M H_2SO_4," *Surface Review and Letters*, vol. 16, no. 01, pp. 49–54, 2009.

[37] N. Hechiche, D. Boughrara, A. Kadri, N. Dahmani, and N. Benbrahim, "Artemisia herba alba essential oil as green corrosion inhibitor for aluminum in hydrochloric acid solution," *Analytical and Bioanalytical Electrochemistry*, vol. 11, pp. 1129–1147, 2019.

[38] A. Berrissoul, E. Loukili, N. Mechbal et al., "Anticorrosion effect of a green sustainable inhibitor on mild steel in hydrochloric acid," *Journal of Colloid and Interface Science*, vol. 580, pp. 740–752, 2020.

[39] B. A. Boukamp, *Equivalent Circuit*, University of Twente, Enschede, Netherlands, 1990.

[40] R. G. Parr and R. G. Pearson, "Absolute hardness: companion parameter to absolute electronegativity," *Journal of the American Chemical Society*, vol. 105, no. 26, pp. 7512–7516, 1983.

[41] A. Khadraoui, A. Khelifa, L. Touafri, H. Hamitouche, and R. Mehdaoui, "Adsorption and Inhibitive Properties of Ruta chalepensis L. Oil as a Green Inhibitor of Steel in 1 M Hydrochloric Acid Medium," *Journal of Materials and Environmental Science*, vol. 4, pp. 663–670, 2013.

[42] C. M. A. Brett, "On the electrochemical behaviour of aluminium in acidic chloride solution," *Corrosion Science*, vol. 33, no. 2, pp. 203–210, 1992.

[43] S. Kshama Shetty and A. Nityananda Shetty, "Eco-friendly benzimidazolium based ionic liquid as a corrosion inhibitor for aluminum alloy composite in acidic media," *Journal of Molecular Liquids*, vol. 225, pp. 426–438, 2017.

[44] C. Trinidad, J. Świątowska, S. Zanna et al., "Effect of surface preparation treatments on copper enrichment on 2024 aluminium alloy surface," *Applied Surface Science*, vol. 560, Article ID 149991, 2021.

[45] J. R. Scully, "Polarization resistance method for determination of instantaneous corrosion rates," *Corrosion*, vol. 56, no. 2, pp. 199–218, 2000.

[46] H. J. W. Lenderink, M. V. D. Linden, and J. H. W. De Wit, "Corrosion of aluminium in acidic and neutral solutions," *Electrochimica Acta*, vol. 38, no. 14, pp. 1989–1992, 1993.

[47] J. Bessone, C. Mayer, K. Jüttner, and W. J. Lorenz, "AC-impedance measurements on aluminium barrier type oxide films," *Electrochimica Acta*, vol. 28, no. 2, pp. 171–175, 1983.

[48] H. J. de Wit, C. Wijenberg, and C. Crevecoeur, "Impedance measurements during anodization of aluminum," *Journal of the Electrochemical Society*, vol. 126, no. 5, pp. 779–785, 1979.

[49] X. Li, S. Deng, and X. Xie, "Experimental and theoretical study on corrosion inhibition of oxime compounds for aluminium in HCl solution," *Corrosion Science*, vol. 81, pp. 162–175, 2014.

[50] N. Ugin Inbaraj and G. Venkatesa Prabhu, "Corrosion inhibition properties of paracetamol based benzoxazine on HCS and Al surfaces in 1M HCl," *Progress in Organic Coatings*, vol. 115, pp. 27–40, 2018.

[51] I. M. Mejeha, M. C. Nwandu, K. B. Okeoma et al., "Experimental and theoretical assessment of the inhibiting action of Aspilia africana extract on corrosion aluminium alloy AA3003 in hydrochloric acid," *Journal of Materials Science*, vol. 47, no. 6, pp. 2559–2572, 2012.

[52] L. Garrigues, N. Pebere, and F. Dabosi, "An investigation of the corrosion inhibition of pure aluminum in neutral and acidic chloride solutions," *Electrochimica Acta*, vol. 41, no. 7-8, pp. 1209–1215, 1996.

[53] D. D. Do, *Adsorption Analysis: Equilibria and Kinetics*, Imperial College Press, London, UK, 1998.

[54] V. C. Srivastava, I. D. Mall, and I. M. Mishra, "Equilibrium modeling of ternary adsorption of metal ions onto rice husk ash," *Journal of Chemical and Engineering Data*, vol. 54, no. 3, pp. 705–711, 2009.

[55] E. I. Ating, S. A. Umoren, I. I. Udousoro, E. E. Ebenso, and A. P. Udoh, "Leaves extract of*Ananas sativum*as green corrosion inhibitor for aluminium in hydrochloric acid solutions," *Green Chemistry Letters and Reviews*, vol. 3, no. 2, pp. 61–68, 2010.

[56] F. M. Donahue and K. Nobe, "Theory of organic corrosion inhibitors," *Journal of the Electrochemical Society*, vol. 112, no. 9, p. 886, 1965.

[57] A. Kokalj, "Corrosion inhibitors: physisorbed or chemisorbed?" *Corrosion Science*, vol. 196, Article ID 109939, 2022.

[58] A. El Bribri, M. Tabyaoui, B. Tabyaoui, H. El Attari, and F. Bentiss, "The use of Euphorbia falcata extract as eco-friendly corrosion inhibitor of carbon steel in hydrochloric acid solution," *Materials Chemistry and Physics*, vol. 141, no. 1, pp. 240–247, 2013.

[59] M. Srivastava, P. Tiwari, S. K. Srivastava, A. Kumar, G. Ji, and R. Prakash, "Low cost aqueous extract of Pisum sativum peels for inhibition of mild steel corrosion," *Journal of Molecular Liquids*, vol. 254, pp. 357–368, 2018.

[60] J. Haque, C. Verma, V. Srivastava, and W. W. Nik, "Corrosion inhibition of mild steel in 1M HCl using environmentally benign Thevetia peruviana flower extracts," *Sustainable Chemistry and Pharmacy*, vol. 19, Article ID 100354, 2021.

[61] L. Valek and S. Martinez, "Copper corrosion inhibition by Azadirachta indica leaves extract in 0.5 M sulphuric acid," *Materials Letters*, vol. 61, no. 1, pp. 148–151, 2007.

[62] S. S. de Assunção Araújo Pereira, M. M. Pêgas, T. L. Fernández et al., "Inhibitory action of aqueous garlic peel extract on the corrosion of carbon steel in HCl solution," *Corrosion Science*, vol. 65, pp. 360–366, 2012.

[63] H. Ashassi-Sorkhabi, B. Shabani, B. Aligholipour, and D. Seifzadeh, "The effect of some Schiff bases on the corrosion of aluminum in hydrochloric acid solution," *Applied Surface Science*, vol. 252, no. 12, pp. 4039–4047, 2006.

[64] M. Bouklah, N. Benchat, A. Aouniti et al., "Effect of the substitution of an oxygen atom by sulphur in a pyridazinic

molecule towards inhibition of corrosion of steel in 0.5M H2SO4 medium," *Progress in Organic Coatings*, vol. 51, no. 2, pp. 118–124, 2004.

[65] O. L. Riggs Jr. and R. M. Hurd, "Temperature coefficient of corrosion inhibition," *Corrosion*, vol. 23, no. 8, pp. 252–260, 1967.

[66] W. Durnie, R. De Marco, A. Jefferson, and B. Kinsella, "Development of a structure-activity relationship for oil field corrosion inhibitors," *Journal of the Electrochemical Society*, vol. 146, no. 5, pp. 1751–1756, 1999.

[67] A. Boag, A. E. Hughes, N. C. Wilson et al., "How complex is the microstructure of AA2024-T3?" *Corrosion Science*, vol. 51, no. 8, pp. 1565–1568, 2009.

[68] A. Bertella, K. Benlahcen, S. Abouamama et al., "Artemisia herba-alba Asso. essential oil antibacterial activity and acute toxicity," *Industrial Crops and Products*, vol. 116, pp. 137–143, 2018.

[69] R. Belhattab, L. Amor, J. G. Barroso, L. G. Pedro, and A. Cristina Figueiredo, "Essential oil from Artemisia herba-alba Asso grown wild in Algeria: variability assessment and comparison with an updated literature survey," *Arabian Journal of Chemistry*, vol. 7, no. 2, pp. 243–251, 2014.

[70] T. Souhila, B. Fatma Zohra, and H. S. Tahar, "Identification and quantification of phenolic compounds of *Artemisia herba-alba* at three harvest time by HPLC–ESI–Q-TOF–MS," *International Journal of Food Properties*, vol. 22, no. 1, pp. 843–852, 2019.

[71] A. A. Ahmed, M. Abou-El-Ela, J. Jakupovic, A. A. S. El-Din, and N. Sabri, "Eudesmanolides and other constituents from Artemisia herba-alba," *Phytochemistry*, vol. 29, no. 11, pp. 3661–3663, 1990.

[72] N. A. M. Saleh, S. I. El-Negoumy, and M. M. Abou-zaid, "Flavonoids of Artemisia judaica, A. Monosperma and A. herba-alba," *Phytochemistry*, vol. 26, no. 11, pp. 3059–3064, 1987.

[73] H. Ashassi-Sorkhabi, Z. Ghasemi, and D. Seifzadeh, "The inhibition effect of some amino acids towards the corrosion of aluminum in 1M HCl+1M H2SO4 solution," *Applied Surface Science*, vol. 249, no. 1-4, pp. 408–418, 2005.

[74] H. Tang, J. Sun, D. Su, Y. Huang, and P. Wu, "Coumarin as a green inhibitor of chloride-induced aluminum corrosion: theoretical calculation and experimental exploration," *RSC Advances*, vol. 11, no. 40, pp. 24926–24937, 2021.

[75] P. C. Okafor, V. E. Ebiekpe, C. F. Azike, G. E. Egbung, E. A. Brisibe, and E. E. Ebenso, "Inhibitory action of*Artemisia annua*extracts and artemisinin on the corrosion of mild steel in H_2SO_4Solution," *International Journal of Corrosion*, vol. 2012, Article ID 768729, 8 pages, 2012.

[76] M. Lebrini, F. Suedile, P. Salvin et al., "Bagassa guianensis ethanol extract used as sustainable eco-friendly inhibitor for zinc corrosion in 3% NaCl: electrochemical and XPS studies," *Surfaces and Interfaces*, vol. 20, Article ID 100588, 2020.

[77] A. Kokalj, "Electrostatic model for treating long-range lateral interactions between polar molecules adsorbed on metal surfaces," *Physical Review B: Condensed Matter*, vol. 84, no. 4, Article ID 45418, 2011.

[78] K. Aramaki, T. Mochizuki, and H. Nishihara, "Effect of chloride ion on the relationship between the adsorption of polar organic compounds on nickel or iron and the HSAB principle," *Journal of the Electrochemical Society*, vol. 135, no. 10, pp. 2427–2432, 1988.

[79] L. Dangleterre, J.-P. Cornard, and C. Lapouge, "Spectroscopic and theoretical investigation of the solvent effects on Al(III)–hydroxyflavone complexes," *Polyhedron*, vol. 27, no. 6, pp. 1581–1590, 2008.

[80] R. G. Buchheit, R. P. Grant, P. F. Hlava, B. Mckenzie, and G. L. Zender, "Local dissolution phenomena associated with S phase (Al2CuMg) particles in aluminum alloy 2024-T3," *Journal of the Electrochemical Society*, vol. 144, no. 8, pp. 2621–2628, 1997.